Ice-covered Environmental Adaptability Assessment for Overhead Contact System in High-speed Railways*

Huan Zhang[1], *Wenfu Wei*[1, 2*], *Like Pan*[3], *Zefeng Yang*[1], *Guizao Huang*[1], *Yuxin Liu*[1], *Xing Chen*[1], *Ziqian Yang*[1] *and Guangning Wu*[1]

(1. School of Electrical Engineering, Southwest Jiaotong University, Chengdu 611756, China;
2. National Rail Transit Electrification and Automation Engineering Technology Research Center, Southwest Jiaotong University, Chengdu 611756, China;
3. China Academy of Railway Sciences Corporation Limited, Beijing 100000, China)

Abstract: High-speed trains rely on pantograph-catenary systems (PCSs) to collect electrical energy from power systems. However, the dynamic interaction between the pantograph and the catenary system may become mismatched once ice accumulates on the overhead conductors. More frequent arcing may occur within the PCS during train operation, posing an unpredictable threat to operational safety. Therefore, it is crucial to evaluate the ability of overhead contact system (OCS) to withstand ice-covered variability during line desgin. A new strategy is proposed to evaluate the adaptive performance of an OCS under various icing conditions. First, a dynamic model considering icing conditions is constructed to simulate the interaction within the PCS. Five different OCS structures with various icing thicknesses are studied. The parameters of the contact force within the PCS and proportion of high-possibility arcing moments are obtained. The dependence of the contact force on the icing thickness and pantograph displacement has been illustrated in the form of cloud maps. Finally, the OCS sensitivity coefficient is calculated, and ice-covered environmental adaptability assessments for the five different OCS structures are compared.

Keywords: Overhead contact system, environmental adaptability, sensitivity coefficient, icing thickness, contact force

1 Introduction

The overhead contact system (OCS) is a key component of electrified railways. High-speed trains constantly collect electrical energy through the sliding friction between the pantograph and the OCS [1-2]. The current collection process is complex and depends on electrical relationships, material properties, and intense mechanical interactions [3-4]. As the OCS is an elastic structure with changing stiffness, during train operation, the contact wire suffers from lifting, deformation, and vibration by the pantograph to varying degrees [5]. This can result in fluctuations in the contact force (CF) within the pantograph-catenary system (PCS) [6-7], which can directly influence the current collection quality of the train [8-9].

As high-speed railway networks are rapidly increasing, OCSs along railway lines will inevitably be installed in complex geographical conditions and may suffer extremely harsh weather conditions. In exceedingly cold and highland regions, the surface of the OCS can be covered with ice under freezing and humid weather conditions [10]. For instance, the Moscow-Kazan high-speed railway may experience winter temperatures as low as –48 ℃, causing ice accumulation of up to 15 mm on the OCS. Similarly, the Sichuan-Tibet railway in China's southwest plateau region can be severely affected by ice accumulation of up to 20 mm. Therefore, it is necessary to focus on the ice-covered conditions of the OCS.

The influence of OCS icing on the pantograph-catenary interaction and current collection performance is illustrated in Fig. 1. Fig. 1a shows a

Manuscript received December 5, 2023; revised February 19, 2024; accepted March 1, 2024. Date of publication June 30, 2024; date of current version March 21, 2024.
* Corresponding Author, E-mail: wfwei@home.swjtu.edu.cn
* Supported by China State Railway Group Co., Ltd. (L2022G006), Chengdu Guojia Electrical Engineering Co., Ltd. (NEEC-2022-A04), and Natural Science Foundation of Sichuan Province (2022NSFSC1863).
Digital Object Identifier: 10.23919/CJEE.2024.000058

photograph of the high-speed train and key components of the OCS under ice-covered conditions. These key components include the contact wire, messenger wire, dropper, and steady arm. The contact wire fluctuation in the figure is a result of the dynamic interaction within the PCS.

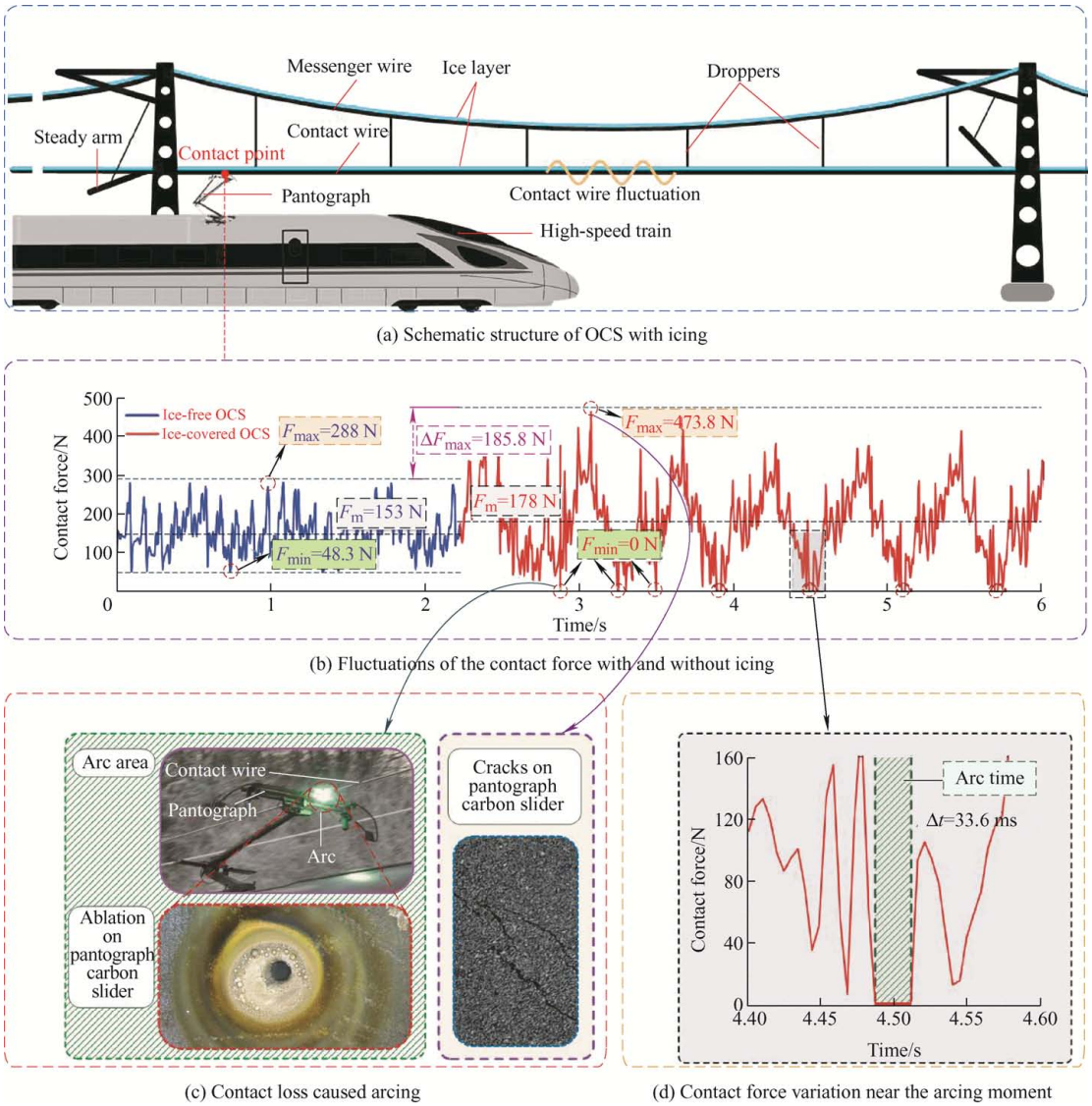

Fig. 1 Influence of ice-covered condition on PCS

Once ice accumulates on overhead conductors, the dynamic interaction becomes more drastic. The change in contact force between the PCS over time is illustrated in Fig. 1b. Evidently, the CF of the ice-covered OCS fluctuates more dramatically than that of the ice-free OCS. An obvious difference exists between the maximum and minimum contact forces. In addition, the mean contact force increases significantly. Owing to the increased sag of the line caused by the ice coating, the stiffness distribution becomes more uneven. Consequently, the fluctuations in the contact force within the PCS will be more drastic. Furthermore, relevant tests and research have confirmed that the stability of the contact line is reduced with an increase in icing thickness [11-12]. Therefore, when the train enters the ice-covered wire area, it is difficult to maintain a continuous dynamic stability between the PCS. Fig. 1c shows that after the loss of stable interaction within the PCS, an excessively high CF may result in cracks on the pantograph carbon slider, whereas an exceedingly low CF increases the possibility of an arc and causes ablation on the pantograph carbon slider. Fig. 1d shows that the pantograph separates from the contact line after the train passes the ice-covered OCS, and the system experiences a longer arcing time [13-14]. Related research has also shown that an increase in icing thickness aggravates damage to the OCS and affects

the current collection quality of trains [15]. In brief, the ice-covered OCS causes the vibration to become elusive, and the coupling relationship between the PCS deteriorates significantly [16]. At present, it is well accepted that the icing on the OCS has a significant influence on current collection quality. However, the performances of different OCS structures under different icing conditions are still lacking and require a systematic and detailed investigation.

In this study, a new strategy is proposed to evaluate the adaptive performance of an OCS under various icing conditions. A dynamic model that considers icing conditions is constructed. Five different OCS structures with various ice thicknesses are studied. The parameters of the contact force within the PCS and proportion of high-possibility arcing moments were obtained. The dependence of the contact force on the icing thickness and pantograph displacement is illustrated. Finally, the OCS sensitivity coefficient is calculated, and the adaptability assessments for five different OCS structures are compared.

2 Establishing dynamic model of PCS

2.1 The coupled model of pantograph-catenary

Adopting the finite element method to define the OCS components and obtain their geometric models [17], the Euler-Bernoulli beam is used to model the contact wire, messenger wire, and dropper [18], a nonlinear rod unit is selected for the steady arm [19], and the mass unit is used to simulate some additional parts, such as the dropper clip. The mass, damping, and stiffness matrices of the OCS are obtained after the mesh division, and a differential equation is established as follows

$$\boldsymbol{M}_c\boldsymbol{u}_c'' + \boldsymbol{C}_c\boldsymbol{u}_c' + \boldsymbol{K}_c\boldsymbol{u}_c = \boldsymbol{f}(t) \tag{1}$$

In Eq. (1), $\boldsymbol{M}_c$, $\boldsymbol{C}_c$, and $\boldsymbol{K}_c$ represent the mass, damping, and stiffness matrices of the OCS, respectively; $\boldsymbol{u}_c''$, $\boldsymbol{u}_c'$, and $\boldsymbol{u}_c$ represent the node acceleration, velocity, and displacement matrices, respectively; and $\boldsymbol{f}(t)$ is the expressed point-load matrix.

The deformation displacement of the messenger and contact wires under the influence of gravity is calculated using the separate model method. During the construction of the OCS, the tension of each dropper at the connection point can be determined based on the weight of the wire, position of the dropper, and pre-sag of the catenary. These tensions are then applied to the messenger wire to obtain the initial displacement of the wire and the length of the dropper that satisfies mechanical equilibrium [20]. Finally, the static equilibrium state of the overhead contact line is solved. Generally, the pantograph head, upper frame, and lower frame can be modeled as mass-stiffness-damping systems [21]. The parameter k_c is introduced to simulate the contact stiffness between the PCS, and CF is calculated using a penalty function [22]. Considering the timeliness of the simulation calculation, an ice load is applied to the OCS using an equivalent acceleration method [23-24].

Fig. 2 illustrates the coupled model of the PCS, which includes a three-mass model of the pantograph and a local magnification graph that depicts the interaction of the PCS. The equation of motion is expressed by Eq. (2)

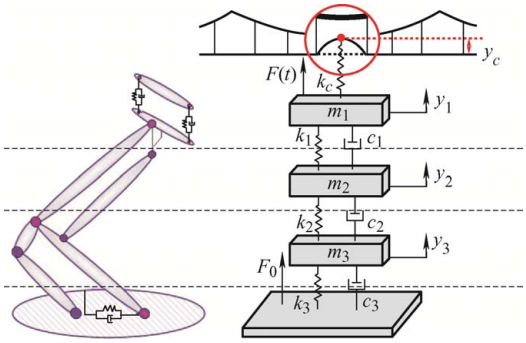

Fig. 2 Coupled model of pantograph-catenary system

$$\begin{cases} m_1\ddot{y}_1 + c_1(\dot{y}_1 - \dot{y}_2) + k_1(y_1 - y_2) = -F(t) \\ m_2\ddot{y}_2 + c_1(\dot{y}_2 - \dot{y}_1) + c_2(\dot{y}_2 - \dot{y}_3) + k_1(y_2 - y_1) + \\ k_2(y_2 - y_3) = 0 \\ m_3\ddot{y}_3 + c_2(\dot{y}_3 - \dot{y}_2) + c_3\dot{y}_3 + k_2(y_3 - y_2) + k_3y_3 = F_0 \end{cases} \tag{2}$$

In Eq. (2), m_i, c_i, and k_i are the pantograph model parameters (i =1, 2, 3); y_i, $\dot{y}_i$, and $\ddot{y}_i$ represent the displacement, velocity, and acceleration of the mass block, respectively; F_0 and $F(t)$ represent the static lifting force and contact force, respectively. The contact force is calculated as follows

$$F(t) = \begin{cases} k_c(y_1 - y_c) & y_1 > y_c \\ 0 & y_1 < y_c \end{cases} \tag{3}$$

In Eq. (3), the vertical displacement of the contact

line element at the contact point is denoted by y_c.

2.2 Model verification

Based on the PCS simulation parameters outlined in the latest EN50318:2018 publication [25], which provides detailed parameter values for PCS (the specific parameter values are provided in Tab. 1), a 10-span OCS model was constructed with 200 m between the two pantographs.

Tab. 1 Key parameter values for pantograph-catenary system

Pantograph-catenary system		Parameter
Structural parameters of overhead contact system	Contact line	Tension=22 kN; Density=1.35 kg/m; Young's modulus=100 kN/mm^2; Cross section=150 mm^2
	Messenger	Tension=16 kN; Density=1.08 kg/m; Young's modulus=97 kN/mm^2; Cross section=120 mm^2
	Dropper	Clamp on contact wire=0.195 kg; Clamp on messenger wire=0.165 kg; Number of droppers per span=9; The position of droppers within each span(m): 4.5; 10.25; 16.0; 21.75; 27.50; 33.25; 39.00; 44.75; 50.50
	Steam arm	Number of steady arms per support=1; Length=1.2 m;
	Others	Density=0.73 kg/m; Mass of clamp=0 kg Encumbrance=1.2 m; Stagger value=0.2 m; Length of span=55 m
Structural parameters of pantograph	Pantograph head	m_1=7.5 kg; c_1=45 Ns/m; k_1=7 000 N/m
	Upper frame	m_2=9.0 kg; c_2=0.1 Ns/m; k_2=15 500 N/m
	Lower frame	m_3=6.0 kg; c_3=100 Ns/m; k_3=160 N/m

The CF of the simulation result was calculated at speeds of 275 km/h and 320 km/h and then compared with the standard range after filtering. A comparison of the results is presented in Tabs. 2 and 3, thereby confirming the accuracy of the modeling method and the effectiveness of the dynamic model.

Tab. 2 Speed=275 km/h

Parameter	Standard range		Simulation result	
Pantograph	1	2	1	2
F_m/N	141.5-146.5		142.8	144.1
σ/N	31.9-34.8	50.0-54.5	33.5	52.4
σ(0-5 Hz)	26.4-28.9	41.2-45.4	28.2	42.0
σ(5-20 Hz)	16.2-22.4	25.2-34.7	21.1	32.6
F_{max}/N	219-244	241-290	239.9	283.0
F_{min}/N	71-86	14-50	71.8	39.9

Tab. 3 Speed=320 km/h

Parameter	Standard range		Simulation result	
Pantograph	1	2	1	2
F_m/N	166.5-171.5		166.5	167.0
σ/N	49.5-62.9	30.2-43.8	55.3	42.8
σ(0-5 Hz)	38.7-44.4	14.3-23.3	40.4	22.2
σ(5-20 Hz)	29.0-46.2	26.7-38.2	29.2	37.0
F_{max}/N	295-343	252-317	326.9	264.2
F_{min}/N	55-82	21-86	66.5	27.3

3 Sensitivity evaluate for diverse OCS in iced environment

3.1 Influence of ice-covered on varying OCS

The variation in the overall structure of the OCS leads to differences in the PCS coupling. Thus, it is necessary to explore the changes in the contact force between PCS at various icing thicknesses.

To this end, the model established in Section 2 of this study was used to calculate the CF of the PCS with different icing thicknesses in the five OCS models. Fig. 3 displays the span length, dropper

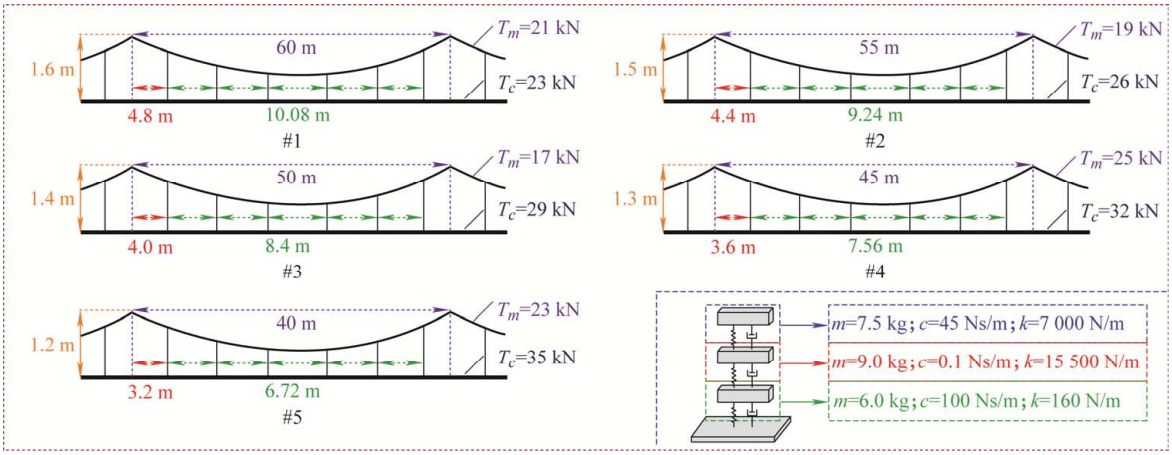

Fig. 3 Five structures of OCS model and pantograph parameters

position, clue tension, and structural height of the five OCS models, labeled #1 to #5. In Fig. 3, T_m and T_c represent the tensions of the messenger and contact wires, respectively. Additionally, a pantograph equivalent model is presented, along with its mass, stiffness, and damping parameters.

As shown in Fig. 3, structure #1 with 11 spans was established, and the CF of the PCS operation was calculated under 0-20 mm icing thickness. To avoid boundary effects, the CF data within 3-9 spans were used to draw the cloud map, and the results are shown in Fig. 4. The color variation represents the different values of CF; the support area has a large CF, and the middle of the span exists in the high-possibility arc area caused by an exceedingly low CF between the PCS. It can be visually seen that the diagram shows a periodic color alternation, which indicates that the CF of the same OCS changes periodically under different icing thicknesses. This is owing to the periodic arrangement of the support installations and droppers within the span during train operation.

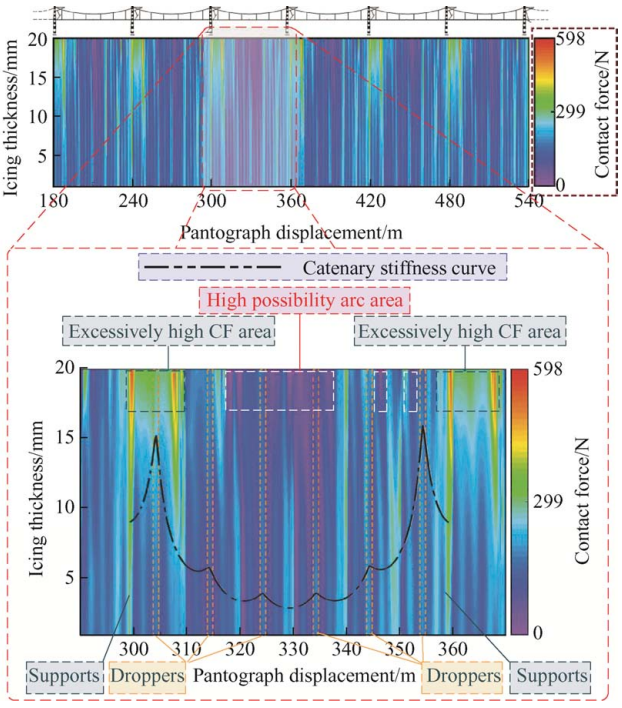

Fig. 4 Contact force vs. pantograph displacement at different icing thicknesses

Considering the CF data within the span when the train's pantograph passes through 300-360 m, the CF data within the span show large values on both sides and small values in the middle, which is consistent with the OCS stiffness distribution. As the OCS stiffness in the middle of the span is too small, the contact line vertical displacement is too large; therefore, the possibility of an arc is higher. The local maximum of the CF is consistent with the location of the supports and droppers circled in the figure, where the rate of change in the stiffness is the greatest [26].

From a vertical perspective, as the thickness of ice increases, the contrast between the light and dark colors becomes more pronounced. This results in a more intense fluctuation in the CF and an increase in the local value of the CF at the supports and droppers. In addition, the possibility of an arc increases.

When differences exist in the OCS structure, the fluctuation of the PCS CF during the train operation varies. Fig. 5 illustrates the CF figure under the #1-#5 OCS for icing thicknesses ranging from 0-20 mm. The CF curve is plotted using data from icing thicknesses of 5 mm, 10 mm, and 20 mm.

Intuitively, the range in which the #1-#5 CF color scales are located continuously decreases. The absolute maximum that occurs near the supports with the most significant stiffness changes are as follows: 597.6 N, 538.6 N, 435.1 N, 375.8 N, and 368.7 N.

In the figure on the left, when observing the structures from #1 to #5, the color change of the contact force becomes smoother as the displacement increases, and the CF value of the corresponding curve on the right continues to converge toward the middle, indicating that the degree of CF fluctuation diminishes. With a slight 5 mm ice-covered condition, the respective values for #1 to #5 F_{m} are 154.4 N, 154.9 N, 155.4 N, 156.6 N, and 156.1 N. For the severe 20 mm ice-covered condition, the F_{m} values are 187.6 N, 180.9 N, 175.1 N, 169.0 N, and 166.8 N. The proportion of dark areas gradually decreases, and the high possibility arc area per hundred meters on the right three curves is 14.6 m, 12.7 m, 10.1 m, 8.6 m, 7.5 m, it means that the probability of arc is reduced.

A comparison of the above indicators is presented in Tab. 4.

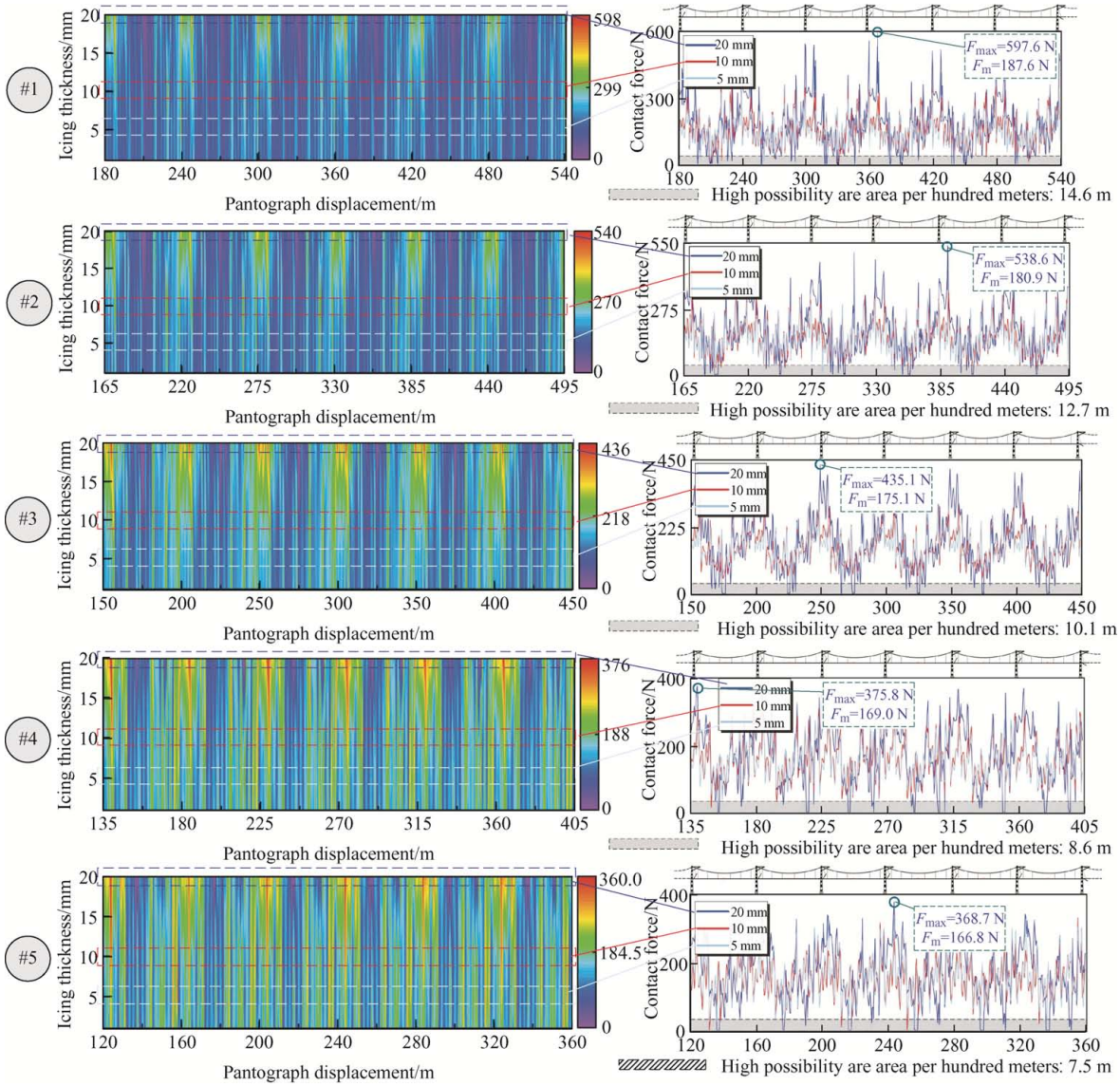

Fig. 5 CF of #1-#5 OCS with varying icing thicknesses

Tab. 4 Comparison of detailed indicators under different overhead contact system

Indicators		#1 result	#2 result	#3 result	#4 result	#5 result
Icing thickness 5 mm	F_{max}/N	353.6	325.3	304.3	308	320.2
	F_m/N	154.4	154.9	155.4	156.6	156.1
	High possibility arc area per hundred meters/m	2.2	1.2	0	0	0
Icing thickness 20 mm	F_{max}/N	597.6	538.6	435.1	375.8	368.7
	F_m/N	187.6	180.9	175.1	169	166.8
	High possibility arc area per hundred meters/m	9.8	8.6	7.8	7.1	6.8

However, the above indicators are insufficient to reflect the adaptability of OCS to the environment, and further analysis of CF data is required.

3.2 Sensitive coefficient of OCS

To better evaluate the adaptability of different OCS to the environment, an evaluation method is required to quantitatively judge the adaptability of a structure to the environment in terms of the numerical magnitude. Accordingly, F_m, F_{max}, F_{min} and σ are used to judge the PCS coupling condition from the perspective of CF [27]. However, while these statistical values can indicate the coupling status of OCS in a specific environment, they do not quantitatively reflect the anti-interference

capacity. Moreover, these values do not facilitate a quantitative comparison and analysis of the sensitivity levels of various OCS.

Consequently, drawing inspiration from the engineering practices used to evaluate the sensitivity of the system output to changes in parameters or surrounding conditions, we propose the introduction of a sensitivity coefficient for the OCS. This sensitivity coefficient enables the assessment of the degree to which the OCS responds to alterations in external conditions or system parameters. This enhancement in the assessment process contributes significantly to a clearer understanding of OCS adaptability and susceptibility to external influences. The sensitivity coefficient of OCS is defined as follows

$$\text{Sensitivity Coefficient of OCS}=\frac{\text{Output Relative Change Rate}}{\text{Environmental Factors Relative Change Rate}} \tag{4}$$

In this paper, Eq. (4) can be expressed as Eq. (5), where S represents the sensitivity coefficient of OCS, ΔF and Δd represent the amount of change in CF and icing thickness, F and d represent the initial CF and icing thickness when the environment remains as the same conditions.

$$S=\frac{\Delta F / F}{\Delta d / d} \tag{5}$$

To ensure that the outcome of the S calculation in Eq. (5) is not infinitesimal, implying that the icing thickness is not considered as 0 mm, and the OCS sensitivity coefficients of the five OCS at 5 mm, 10 mm, 15 mm, and 20 mm ice cover thicknesses are calculated by choosing the 1 mm case as the basis. The results of these calculations are shown in Fig. 6.

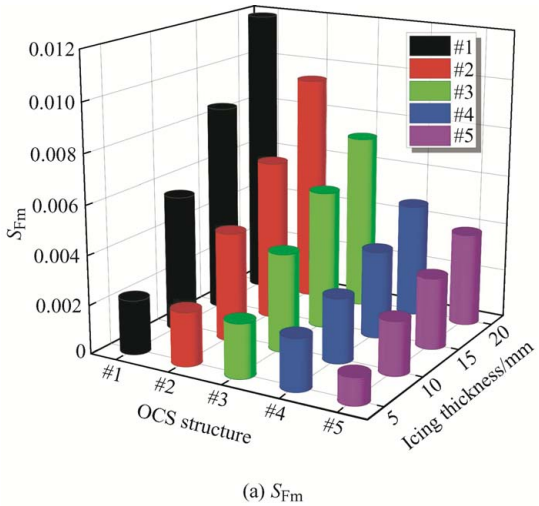

(a) S_{Fm}

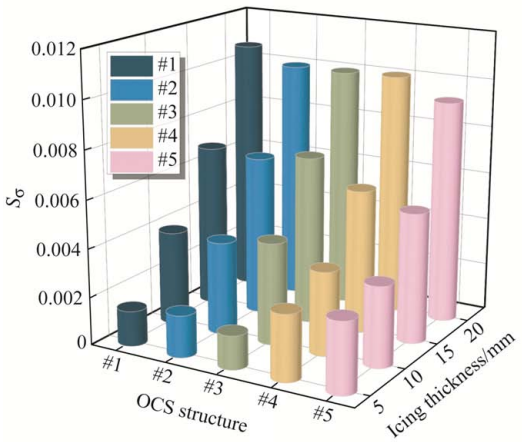

(b) S_σ

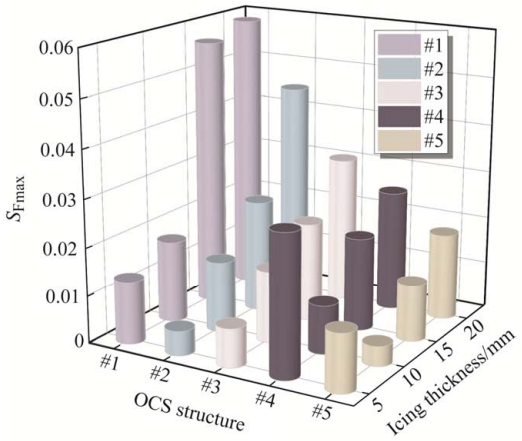

(c) S_{Fmax}

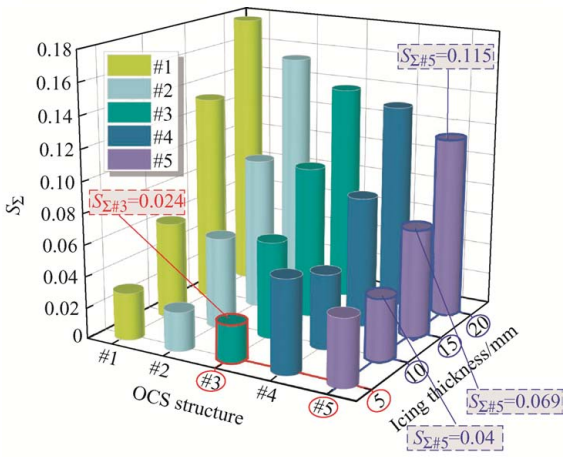

(d) S_Σ

Fig. 6 Sensitivity coefficients of five OCS for different icing thicknesses

The *XOY* plane in the three-dimensional (3D) column diagram indicates the number of OCS structures and icing thickness, and the column height represents the magnitude of the sensitivity coefficient. In Figs. 6a, 6b, and 6c, S_{Fm}, S_σ and S_{Fmax} represent the sensitivity coefficients of the CF statistical value. For the system with stronger environmental adaptability, the sensitivity coefficients regarding each statistical

value of CF under environmental perturbation should be smaller; therefore, the S_Σ obtained by summing S_{Fm}, S_σ and S_{Fmax} is considered the final sensitivity coefficient of OCS.

The lower the column, the smaller the sensitivity coefficient, indicating greater environmental adaptability of the OCS. From the data presented in Fig. 6d, it is evident that structure #3, with a 5 mm ice cover, exhibits higher adaptability, as indicated by $S_{\Sigma\#3}$=0.024. This value is 59.32% lower than that of the less adaptable structure #4 under the same conditions, with $S_{\Sigma\#4}$=0.059. Similarly, structure #5, under a 10 mm ice cover, displays improved adaptability with $S_{\Sigma\#5}$=0.040, which is lower compared to $S_{\Sigma\#1}$=0.062 by 35.48%. Under a 15 mm ice cover, structure #5 continues to demonstrate higher adaptability with $S_{\Sigma\#5}$=0.069, which is 48.12% lower compared to $S_{\Sigma\#1}$=0.133. Moreover, structure #5, covered by 20 mm of ice, maintains greater adaptability with $S_{\Sigma\#5}$=0.115, which is 35.39% lower compared to $S_{\Sigma\#1}$=0.178.

Fig. 7 illustrates the proportion of high-possibility arc times within the four distinct ice environments.

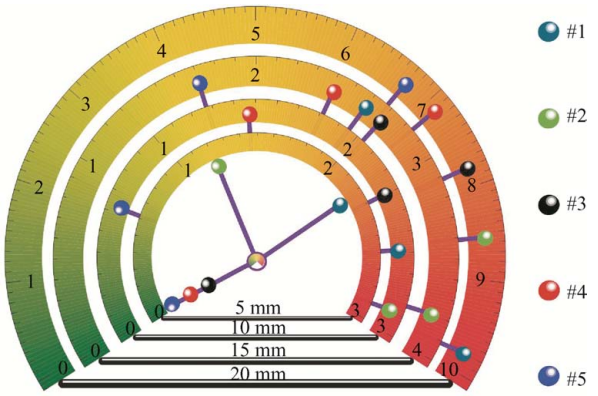

Fig. 7 Proportion of high-possibility arc time (%)

Overall, the adaptability of the different structures to ice-covered environments varied. Structure #1 has the worst adaptability to the ice-covered environment, its S_Σ and the proportion of high possibility arc time are higher. On the other hand, under the slightly ice-covered condition with an icing thickness of 5 mm, structure #3 has the lowest sensitivity coefficient of $S_{\Sigma\#3}$=0.024, and the proportion of high possibility arc time is 0%, which has the strongest ice-resistance performance under the low ice-covered condition. However, as the icing thickness increases, its S_Σ and the proportion of high possibility arc time are larger than #5. When the icing thickness is more than 5 mm until 20 mm, structure #5 reflects its superior anti-icing performance, and it has strong adaptability in each different degree of iced environment, with lower values of S_Σ and the high possibility arc time.

4 Conclusions

Ice-covered conditions may result in a serious mismatch between the pantograph-catenary system, threatening the current collection safety of high-speed railways. Focusing on this problem, we constructed a dynamic model capable of considering icing conditions to explore the interactions within the pantograph-catenary system. Five types of OCS structures were considered and their performances under different icing thickness conditions were compared. We also introduced an OCS sensitivity coefficient to quantitatively assess the environmental adaptability of an overhead contact system. Calculation results indicated that the S_Σ of #3 at 5 mm, 10 mm, 15 mm, and 20 mm icing thickness are 0.02, 0.06, 0.10, and 0.14; the proportion of high possibility arc time is 0%, 2.28%, 2.67%, and 7.80%. Structure #5 at 5 mm, 10 mm, 15 mm, and 20 mm icing thicknesses were 0.04, 0.04, 0.07, and 0.12, respectively; the proportions of high possibility arc time were 0%, 0.67%, 1.67%, and 6.81%, respectively. Overall, under the slightly ice-covered condition with an icing thickness of 5 mm, structure #3 exhibits better environmental adaptability. However, under more severe ice-covered conditions, particularly at higher icing thicknesses, structure #5 exhibits superior environmental adaptability.

References

[1] G Wu, G Gao, W Wei, et al. The current collection approach of high-speed train-pantograph and catenary system, in the electrical contact of the pantograph-catenary system. 1st ed. Singapore: Springer, 2019.

[2] J H Lee, T W Park, H K Oh, et al. Analysis of dynamic interaction between catenary and pantograph with experimental verification and performance evaluation in new high-speed line. *Vehicle System Dynamics*, 2015, 53(8): 1117-1134.

[3] G Wu, W Wei, G Gao, et al. Evolution of the electrical contact of dynamic pantograph-catenary system. *Journal*

of Modern Transportation, 2016, 24(2): 132-138.

[4] Z Yang，B Tang，Y Qiu, et al. Measurement of transient temperature using laser-induced breakdown spectroscopy (LIBS) with the surface temperature effect. *Journal of Analytical Atomic Spectrometry*, 2023, 38(10): 1952-1961.

[5] Z Dai, T Li, N Zhou, et al. Numerical simulation and optimization of aerodynamic uplift force of a high-speed pantograph. *Railway Engineering Science*, 2022, 30(1): 117-128.

[6] A C Hernandez, J D D S Bobi, J G Fernandez, et al. Vibration reduction on overhead contact rails: A simulation-optimization approach. *International Journal of Simulation Modeling*, 2021, 20(2): 315-326.

[7] M Simarro, S Postigo, M Prado-Novoa, et al. Analysis of contact forces between the pantograph and the overhead conductor rail using a validated finite element model. *Engineering Structures*, 2020, 225(2020): 111265.

[8] H Zhou, Z Liu, J Xiong, et al. Characteristic analysis of pantograph-catenary detachment arc based on double-pantograph-catenary dynamics in electrified railways. *IET Electrical Systems in Transportation*, 2022, 12(4): 238-150.

[9] E Chater, D Ghani, F Giri, et al. Output feedback control of pantograph-catenary system with adaptive estimation of catenary parameters. *Journal of Modern Transportation*, 2015, 23(4): 252-261.

[10] G Wu, K Dong, Z Xu, et al. Pantograph-catenary electrical contact system of high-speed railways: Recent progress, challenges, and outlooks. *Railway Engineering Science*, 2022, 30(4): 437-467.

[11] M T Stickland, T J Scanlon. An investigation into the aerodynamic characteristics of catenary contact wires in a cross-wind. *Journal of Rail and Rapid Transit*, 2001, 215(4): 311-318.

[12] M T Stickland, T J Scanlon, I A Craighead, et al. An investigation into the mechanical damping characteristics of catenary contact wires and their effect on aerodynamic galloping instability. *Journal of Rail and Rapid Transit*, 2003, 217(2): 63-71.

[13] W Liu, Y Wang, T Wang, et al. Influence of offline time on the characteristic of arc between pantograph and catenary. *High Voltage Engineering*, 2016, 42(11): 3524-3532.

[14] G Wu, Y Zhou, G Gao, et al. Arc erosion characteristics of Cu-impregnated carbon materials used for current collection in high-speed railways. *IEEE Transactions on Components*, *Packaging and Manufacturing Technology*, 2018, 8(6): 1014-1023.

[15] Y Song, Z Liu, H Wang, et al. Nonlinear analysis of wind-induced vibration of high-speed railway catenary and its influence on pantograph-catenary interaction. *Vehicle System Dynamics*, 2016, 54(6): 723-747.

[16] Z Xu, Y Song, Z Liu. Effective measures to improve current collection quality for double pantographs and catenary based on wave propagation analysis. *IEEE Transactions on Vehicular Technology*, 2020, 69(6): 6299-6309.

[17] International Union of Railways. UIC CODE 799. Characteristics of a.c. overhead contact systems for high-speed lines worked at speeds of over 200 km/h. Paris: International Union of Railways, 2002.

[18] Z Liu, Y Song, Y Han, et al. Advances of research on high-speed railway catenary. *Journal of Modern Transportation*, 2018, 26(1): 1-23.

[19] Y Song, Z Liu, H Wang, et al. Nonlinear modelling of high-speed catenary based on analytical expressions of cable and truss elements. *Vehicle System Dynamics*, 2015, 53(10): 1455-1479.

[20] S Bruni, J Ambrosio, A Carnicero, et al. The results of the pantograph-catenary interaction benchmark. *Vehicle System Dynamics*, 2014, 53(3): 412-435.

[21] Y H Cho, K Lee, Y Park, et al. Influence of contact wire pre-sag on the dynamics of pantograph-railway catenary. *International Journal of Mechanical Sciences*, 2010, 52(11): 1471-1490.

[22] B Zhu, Z Ren, W Xie, et al. Active nonlinear partial-state feedback control of contacting force for a pantograph-catenary system. *ISA Transactions*, 2019, 91: 78-89.

[23] Y Yao, N Zhou, G Mei, et al. Dynamic analysis of pantograph-catenary system considering ice coating. *Shock and Vibration*, 2020, 2020: 1-15.

[24] A Jamaleddine, G McClure, J Rousselet, et al. Simulation of ice-shedding on electrical transmission lines using adina. *Computers & Structures*, 1993, 47(4-5): 523-536.

[25] British Standards Institution. BS EN 50318. Railway applications-Current collection systems-Validation of simulation of the dynamic interaction between pantograph and overhead contact line. London: British Standards Institution, 2018.

[26] J Zhang, W Liu, M Yu, et al. Simulation analysis of

offline characteristics between pantograph and catenary. *IET Electrical Systems in Transportation*, 2017, 7(3): 252-257.

[27] BS EN 50367. Railway applications-Current collection systems-Technical criteria for the interaction between pantograph and overhead line. London: British Standards Institution, 2012.

Huan Zhang was born in Gansu, China, in 1999. He received the B.S. degree in Electrical Engineering and Automation from Anhui University of Science and Technology, Anhui, China, in 2021. He is currently pursuing the M.S. degree with the School of Electrical Engineering, Southwest Jiaotong University, Chengdu, China. His current research interests focus on the simulation study of pantograph-catenary electrical contact.

Wenfu Wei (Senior Member, IEEE) was born in Shandong, China, in 1987. He received the B.Sc. and Ph.D. degrees in Electrical Engineering from Xi'an Jiaotong University, Xi'an, China, in 2010 and 2014, respectively.

He has won the first prize of the Science Progress Award of the Ministry of Education, and is the Chairman of IEEE P2753 Work Group.

His current research interests include the theory and technology of electrical contact, arc plasma, and advanced electrical materials, especially in the fields of power systems and electrified railway.

Like Pan was born in Shaanxi, China, in 1986. He received the Ph.D. degree in Vehicle Operation Engineering for the Beijing Jiaotong University, Beijing, China, in 2017.

His research interests are in the field of electrified railway traction power supply technology and pantograph-catenary coupling technology.

Zefeng Yang (Member, IEEE) was born in Sichuan, China, in 1989. He received the B.S. and Ph.D. degrees in Electrical Engineering from Xi'an Jiaotong University, Xi'an, China, in 2012 and 2017, respectively.

He has won the first prize of the Science Progress Award of the Ministry of Education, for his contributions on the pantograph system of the high speed train.

His current research interests include arc plasma, plasmas application, and plasmas diagnosis.

Guizao Huang was born in Sichuan, China, in 1993. He received the B.S. and Ph.D. degrees in Electrical Engineering from Chongqing University, Chongqing, China, in 2015 and 2020, respectively.

He is a member of CIGRE B2.84 and IEEE P3133 working groups, and his current research interests include dynamic matching characteristics of the pantograph-catenary system, disaster-causing mechanisms and prevention methods for extra-high voltage transmission lines.

Yuxin Liu was born in Hebei, China, in 1998. He received the B.S. degree in Electrical Engineering and Automation from Shanghai Electric Power University, Shanghai, China, in 2021. He is currently pursuing the M.S. degree with the School of Electrical Engineering, Southwest Jiaotong University, Chengdu, China.

His current research interests focus on the study of pantograph-catenary dynamics.

Xing Chen was born in Wuhan, China, in 1998. He received the B.S. degree in Electrical Engineering and Automation from China Three Gorges University, Hubei, China, in 2020. He is currently pursuing the M.S. degree with the School of Electrical Engineering, Southwest Jiaotong University, Chengdu, China.

His current research interests focus on the simulation study of pantograph-catenary electrical contact.

Ziqian Yang was born in Hebei, China, in 2001. She received the B.S. degree in Electrical Engineering and Automation from North China University of Science and Technology, Hebei, China, in 2023. She is currently pursuing the M.S. degree with the School of Electrical Engineering, Southwest Jiaotong University, Chengdu, China.

Her current research interests focus on the simulation study of pantograph-catenary dynamics.

Guangning Wu (Fellow, IEEE) was born in Nanjing, China, in 1969. He received the B.Sc., M.Sc., and Ph.D. degrees in Electrical Engineering from Xi'an Jiaotong University, Xi'an, China, in 1991, 1994, and 1997, respectively.

His research interests include electric arc, rail transit power supply, high voltage, and insulation technology for electrical equipment.

Prof. Wu is a Distinguished Professor of Cheung Kong Scholar. He was a recipient of the National Science Fund for Distinguished Young Scholars.